High Occurrence Optical Spikes and Quasi-Periodic Pulses (QPPs) on X-ray Star 47 Cassiopeiae

Gary Vander Haagen
Stonegate Observatory, 825 Stonegate Road, Ann Arbor, MI 48103; garyvh2@gmail.com

Received May 6, 2019; revised July 23, 2019; accepted September 9, 2019

Abstract The high cadence flare search of X-ray star 47 Cas revealed 46 B-band flares at 0.26 to 0.78 mag peak above the mean. Durations of the very short flares or spikes ranged from 20 to 220 ms and energy levels from 22.7 to 199.5 × 10^{31} ergs. The study collected 2.6 × 10^{7} photometric measurements over 32.3 hours from October 19, 2018, through April 9, 2019. The 46 flares identified represent a flare rate of 4.6 flares/hour during the 500 samples/sec sampling period. The analysis showed numerous quasi-periodic pulses (QPPs) accompanying the spikes, with the most predominant frequencies of 2 to 12 Hz.

1. Introduction

47 Cas is a type F0V, high proper motion, high luminosity X-ray star with B-mag 5.590, V-mag 5.268, and parallaxes of 30.16 mas (Wenger *et al.* 2000). Gudel *et al.* (1998) note that 47 Cas has been studied periodically since 1995 for its high X-ray luminosity and for better understanding of stellar evolution in the region between solar type stars beyond F5V and early F-stars. X-ray and microwave data analysis from the same study shows the star is a triple system; 47 Cas A as 1.5 Ms and 47 Cas B as 1.1 Ms with an orbital period (AB) of 1616 days. 47 Cas C was detected in a VLA radio map at 3.6 and 6 cm wavelengths at a distance of 2.5" SE of the binary. No other data have been obtained on the third member. In the latest X-ray study by Pandey and Karmakar (2015), using flare data detected by the XMM-Newton mission, an X-ray flare sequence contained 40 times less energy than the total energy emitted at the flares' peak. A large amount of residual energy was released at other longer wavelengths. Also concluded was that the main source of energy for the flare is the star's strong magnetic field and its release likely occurs within a single coronal loop structure.

At optical wavelengths, photometry conducted by Olsen (1983) consisted of uvby data on A5 to G0 stars brighter than mag 8.3 V. The photometric data are consistent with those published later by Hoffleit and Warren (1995) in the *Bright Star Catalogue*. Neither of these studies did time-series work or looked for flaring events. The AAVSO data archives contain no 47 Cas data. Gudel *et al.* (1998) noted that the Villanova University's Automatic Photometric Telescope (APT) reported some "marginally significant variability over a few hours, and probably some longer-term monthly variations" but no data were published.

The energetic nature of 47 Cas at very short wavelengths and near total lack of photometry made it an intriguing candidate for study. The study boundaries included: 1) collection of high cadence B-band photometric data for detection of possible sub-second or longer flare events, 2) where flares are detected, analysis of the length, peak σ, ΔB-mag, total energy released and, (3) a fast Fourier transform (FFT) analysis to isolate any quasi-periodic pulses (QPPs) or short-term variability.

2. Optical system, data collection, and analysis tools

The optical system consisted of a 43-cm corrected Dall-Kirkham scope, a high-speed silicon photomultiplier (SPM), and a data acquisition system capable of sub-millisecond data collection intervals. The Hamamatsu C13366 series SPM was chosen because it has comparable sensitivity to a standard single channel vacuum photomultiplier yet a more robust mechanical and electrical design with the disadvantage of higher dark counts (Vander Haagen 2012).

The optical system is shown in Figure 1. The incoming beam is split approximately 85/4 with the reflected portion passing through the B-band filter, an f-stop yielding a 57 arc-second field, and onto the SPM detector (Vander Haagen 2017). An integral wide bandwidth pulse amplifier amplifies the SPM signal, producing a 2- to 3-volt pulse of approximately 30 ns for each converted photon. These photon pulses are sent to a PC based data acquisition system, a Measurement Computing (2019) DaqBoard 1000 series, where they are gated and counted based upon the collection rate. A 2-ms gate was used for most of the measurements generating a 500 samples/sec acquisition rate. The balance of the incoming beam passes straight through to a B-band filter and a conventional CCD camera used for initial alignment, guiding, and measurement of both the guide star flux and background flux. Referring to Figure 2, the flux value counts from the target data stream along with GPS 1-second time stamps are recorded in the DAQ Log File by the data acquisition system. The CCD Data and Control stream consists of reference and background flux values plus pixel counts for each guide star sample, typically every 5 seconds. These values are stored in the AG (auto-guider) Tracker Log file.

Upon completion of the night's search the DAQ Log File and the CCD's AG Tracker Log File are merged as shown in Figure 3. The large DAQ Log File with up to1 million data samples is parsed with the much slower occurring auto-guider, AG Tracker Log. Here, every target data point is matched to the time-appropriate Tracker data with the target counts corrected for the SPM dark counts and sky background in a quadrature calculation and each sample GPS time stamped. This parsing operation results in an integrated file or "data set" with all constituents ready for analysis, with the file containing up to 1 million sample lines each containing target, reference, and background data. Files of this size are too large for spreadsheet

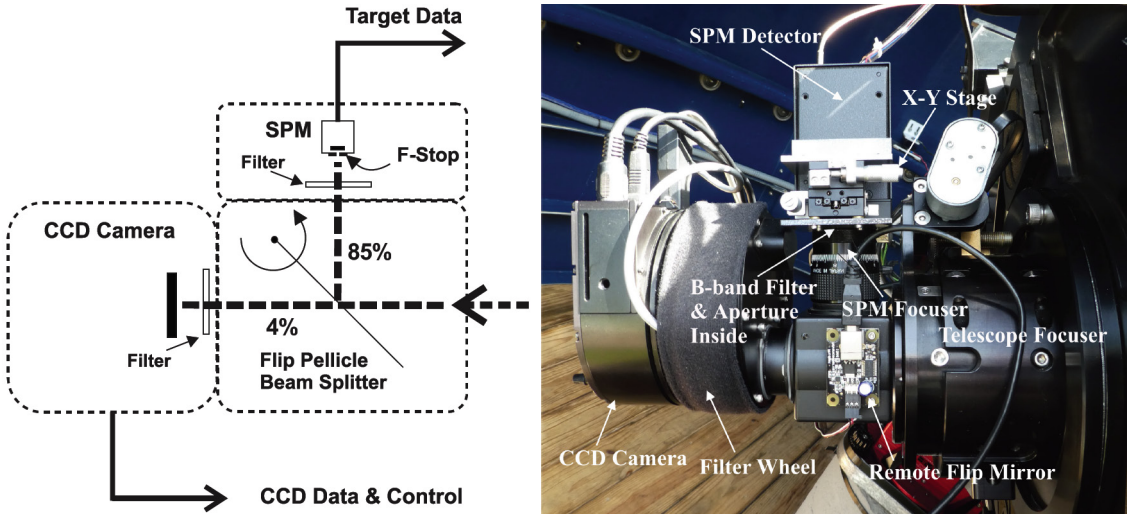

Figure 1. The optical train schematic and photo shows the pellicle beam splitter with both reflected and pass-through beams. The reflected beam passes through the B-band filter, aperture, and onto the silicon photomultiplier (SPM). The pellicle can be flipped to allow 100% light transmission for initial target alignment using the CCD camera. The SPM is mounted on a X–Y stage for precise centering of detector to the centerline of the CCD camera. Guiding is provided with pellicle in position shown. The target SPM photon counts and data from the CCD camera are processed and stored as shown in data acquisition pipeline (Figure 2).

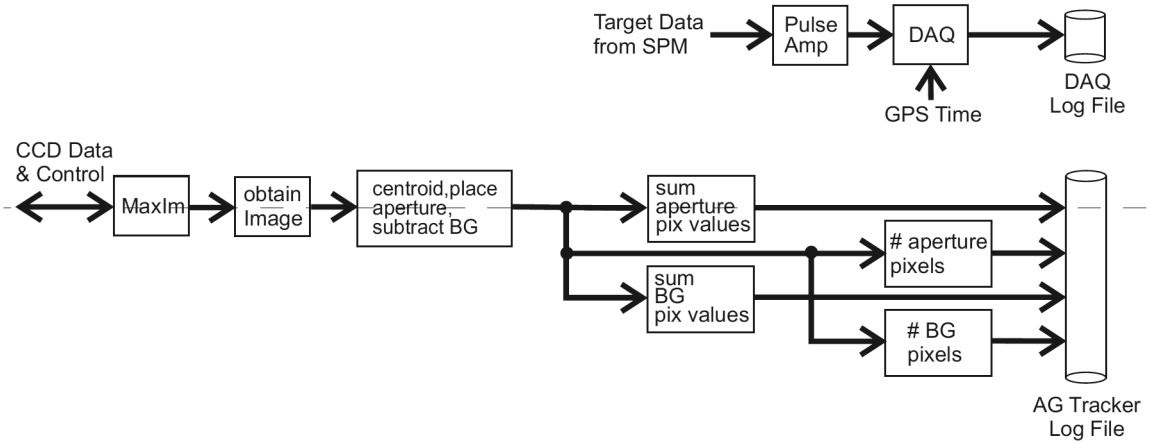

Figure 2. The data acquisition pipeline consists of two streams, the target photon counts and CCD camera image data. The low-level SPM photon counts are amplified and counted by the data acquisition system (DAQ) for the period selected (ex. 2 ms) and the data written to the DAQ Log File. A GPS synced time stamp is added every second to the appropriate data line. The DAQ Log is limited to 1 million data lines per file. The CCD data feeds the camera control program that extracts the guide-star image, centroids the image, and extracts both flux and pixel count for the guide star and background. This occurs at a rate determined by the guide star exposure, typically every 5 seconds. These data are written to the AG Tracker Log File.

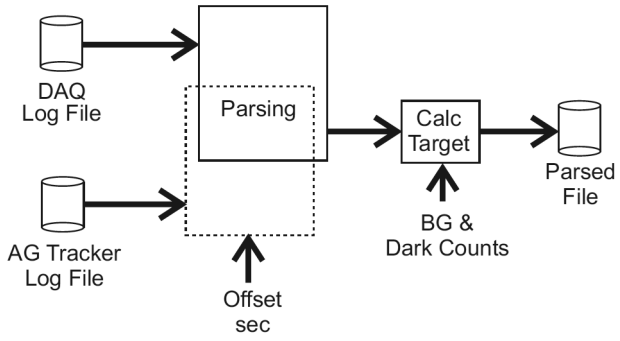

Figure 3. Upon completion of the data collection the DAQ and AG Tracker Log files are merged using a parsing operation. The lower resolution tracker file data are aligned with the DAQ target photon counts, and the target counts are reduced using a quadrature calculation to remove the sky background and SPM dark counts, thereby producing an integrated file of sample by sample target counts, reference star flux, and sky background, all referenced to an accurate UT time stamp in seconds, e.g., 5402 sec equals 1:30:02 UT with resolution to the sample period.

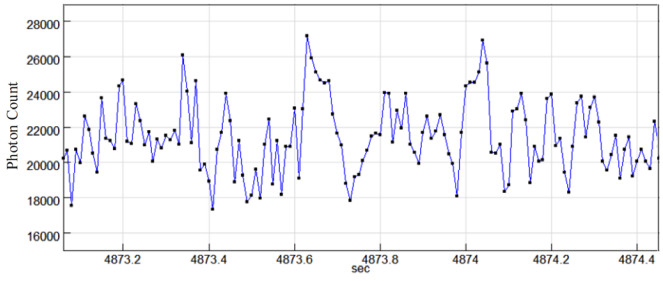

Figure 4. 1/19/2018 flare 1-1.2 is an example of a flare sampled at 10 ms, 100 samples/sec. Note the minimal detail on the rise side of the first large flare at 4873.6 sec reaching 5.8σ and the second flare at 4874.04 sec during the fall period. Such conditions suggest undersampling of the signal.

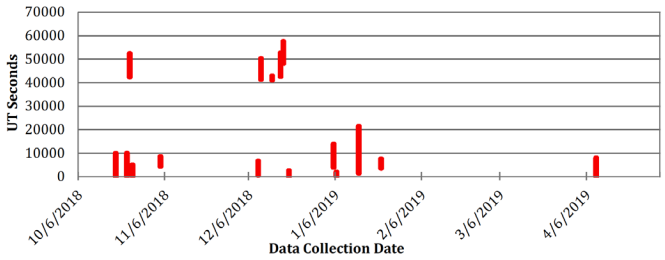

Figure 5. Span of nightly 47 Cas data collection dates. Total data collection time 116.3 Ksec, 32.3 hours.

analysis but are easily analyzed using signal processing software such as SIGVIEW (SignalLab 2019). SIGVIEW 3.2 is capable of quickly handling files up to 10^6 lines of time-based data. Any portion of the data can be reviewed near instantly with a powerful suite of tools: statistical analysis, smoothing, averaging, filtering, resampling, probability distributions, FFTs including spectrograms (FFT segmented over time), and complex calculation capability for correlation and convolution. These data files were reviewed for potential flares using statistical techniques, resampled for better detection and analysis of longer flares, and viewed using digital filters and FFT for detection of possible periodic occurrences.

3. Flare search and data analysis

A criterion was developed to isolate short duration flares in large sample sizes from randomly occurring event sequences (Vander Haagen 2015). A flare must contain a minimum of three consecutive data points, two at or above 3σ and one at or above 5σ. Since the minimum number of photons per gate was always 100 or more, normal distribution statistics were used to compute the standard deviation. Statistics were collected for a minimum 600 seconds prior to the event where possible using digital signal processing software, SIGVIEW 3.2. This process is similar in direction to that followed by flare searches (Byrne *et al.* 1994). The probability of this sequence being a random event can be represented by Equation (1), where N is the number of photons gated each measurement and σ is for the positive events only.

$$\Pi_{3,3,5\sigma} = P_r(3\sigma)^2 5\sigma = (1.35\times10^{-3})^2 \times (2.9\times10^{-7})\,N = 5.2\times10^{-13}\,N \quad (1)$$

With N generally ranging from 4,000 to 5,000 photons per gate at 500 samples/sec the probability of the event sequence being random is approximately 2.5×10^{-9}. This criterion was used for each of the data sets to isolate short duration flares.

Four flares were detected during the 100 samples/sec data collection period October 19, 2018, through January 5, 2019. Figure 4 shows flare 1–1.2 where there is insufficient detail on the rise and fall curves, indicating the flares were sampled at too low a rate. The rate was increased to 500 samples/sec for the data collection runs January 6, 2019, through April 9, 2019. Figure 5 shows the span of nightly data collection times in seconds across the dates. The total data collection time was 32.3 hours or 116.3 Ksec, comprising 2.6×10^7 data points. Table 1 summarizes the 46 flares detected. Four flares were detected at 100 samples/sec or 0.18 flares/hr and 42 flares at 500 samples/sec or 4.6 flares/hr. High cadence studies by Vander Haagen (2017, 2015, 2013) on cooler flare stars have shown much lower flaring activity: CR Dra 0.016 flares/hr (Vander Haagen 2017), BY Dra 0.04 flares/hr (Vander Haagen 2015), and AR Lac

Table 1. Summary of the 47 Cas flare data over the collection period October 19, 2018, through April 9, 2019.

Date	*Flare ID*	*ΔB mag.*	*Peak σ*	*P_b ms*	*E_b ergs $\times 10^{31}$*	*Duration ms*
10/19/2018	1-1.2	0.27	5.8	231.9	199.5	220
10/19/2018	1-2.2	0.26	5.6	95.5	82.1	80
10/23/2018	1-1.1	0.33	5.1	115.1	99.0	100
11/4/2018	1-1.1	0.43	5.5	120.5	103.6	110
1/14/2019	1-1.1	0.33	5.1	95.6	82.3	48
1/14/2019	2-1.3	0.39	5.4	166.8	143.5	104
1/14/2019	2-2.3	0.37	5.1	139.3	119.8	118
1/14/2019	2-3.3	0.37	5.2	69.3	59.6	62
1/14/2019	3-1.2	0.43	6.0	120.5	103.6	102
1/14/2019	3-2.2	0.37	5.1	75.3	64.8	62
1/14/2019	4-1.1	0.37	5.2	97.8	84.1	80
1/14/2019	5-1.1	0.34	5.4	58.0	49.9	48
1/14/2019	6-1.4	0.30	5.1	32.9	28.3	28
1/14/2019	6-2.4	0.34	5.8	71.6	61.5	64
1/14/2019	6-3.4	0.31	5.2	75.1	64.6	64
1/14/2019	6-4.4	0.30	5.0	30.8	26.5	26
1/14/2019	7-1.2	0.29	5.5	173.9	149.5	156
1/14/2019	7-2.2	0.28	5.3	128.9	110.8	112
1/14/2019	8-1.11	0.30	5.1	115.9	99.7	102
1/14/2019	8-2.11	0.42	7.5	84.2	72.4	72
1/14/2019	8-3.11	0.40	7.2	118.9	102.2	102
1/14/2019	8-4.11	0.32	5.5	53.2	45.8	44
1/14/2019	8-5.11	0.30	5.1	40.0	34.4	38
1/14/2019	8-6.11	0.30	5.0	30.6	26.4	30
1/14/2019	8-7.11	0.30	5.1	40.0	34.4	34
1/14/2019	8-8.11	0.37	6.4	96.5	83.0	80
1/14/2019	8-9.11	0.33	5.6	26.4	22.7	20
1/14/2019	8-10.11	0.31	5.3	66.4	57.1	50
1/14/2019	8-11.11	0.30	5.1	59.6	51.3	54
1/14/2019	9-1.3	0.40	6.9	50.8	43.7	38
1/14/2019	9-2.3	0.36	6.1	91.8	78.9	74
1/14/2019	9-3.3	0.33	5.5	132.7	114.1	108
1/14/2019	10.1.2	0.31	5.2	65.3	56.1	86
1/14/2019	10-2.2	0.31	5.2	91.8	78.9	82
1/22/2019	1-1.2	0.49	6.2	68.1	58.6	54
1/22/2019	1-2.2	0.53	7.0	58.3	50.1	46
1/22/2019	2-1.2	0.52	6.9	82.9	71.3	76
1/22/2019	2-2.2	0.54	7.3	40.7	35.0	32
4/9/2019	1-1.3	0.72	5.1	55.5	47.7	40
4/9/2019	1-2.3	0.72	5.0	61.4	52.8	44
4/9/2019	1-3.3	0.73	5.1	90.7	78.0	80
4/9/2019	2-1.3	0.76	5.1	84.0	72.2	64
4/9/2019	2-2.3	0.77	5.1	85.6	73.6	60
4/9/2019	2-3.3	0.78	5.2	48.3	41.5	36
4/9/2019	3-1.2	0.69	5.1	80.5	69.2	58
4/9/2019	3-2.2	0.71	5.3	108.0	92.9	90

0.04 flares/hr, II Peg 0.03 flares/hr, UX Ari 0.04 flares/hr (Vander Haagen 2013), and rarely are any QPPs detected. 47 Cas at 500 samples/sec with 4.6 flares/hr has minimally 100 times the flare rate of those cited.

The median flare duration was 64 ms, ranging from 20 to 220 ms, which is consistent with the studies cited above. The duration was measured between the mean flux value crossings on the rise and fall curve of each flare rounded off to the nearest sample point. The highest flare peak was 7.5σ and largest B-magnitude increase was 0.78.

The energy calculation for each flare starts with conversion of B-band photometric measurements into flux. Equation (2) converts B_0 magnitude into flux (Henden and Kaitchuck 1990):

$$F_b = 10^{-0.4(B_0-q_b)} \text{ watts / (cm}^2 \text{ Angstrom)}, \quad (2)$$

where B_0 is the star's B-mag corrected for atmospheric extinction and q_b is the absolute zero-point constant (Henden and Kaitchuck 1990). Collection of all the radiated star flux within the B-band (BW_b) results in Equation (3) representing the quiescent level for the star:

$$F_b = 4\pi d^2\ 10^{-0.4\,(B_0-q_b)}\ BW_b \text{ watts}. \quad (3)$$

To determine the actual flare flux, Gershberg (1972) computes the "equivalent duration" of a flare, Equation (4):

$$P_b = \int [(I_f - I_0) / I_0]\ dt \text{ sec}. \quad (4)$$

I_f is the flare flux count over the interval dt and I_0 is the quiescent or mean flux count for each data set. Incorporation of the equivalent duration P_b into Equation (3) and conversion from watt-sec to ergs results in the energy level for the flare, Equation (5):

$$E_b = 4\pi d^2\ 10^{-0.4\,(B_0-q_b)}\ BW_b\ 10^7\ P_b \text{ ergs}. \quad (5)$$

Adding the physical properties for 47 Cas results in Equation (6): d = 30.16 mas (Wenger *et al.* 2000) or 1.04 ×10^{20} cm, B_0 = 5.59 (Wenger *et al.* 2000), q_b = –37.86 with the error estimated at 10–20% (Henden and Kaitchuck 1990). The Sloan B-band filter BW_b = 1500 Å (Astrodon 2019). P_b was calculated by numerically integrating in EXCEL each flare's photon count data. The flare energy data along with other key information for each flare are summarized in Table 1.

$$E_b = 8.6 \times 10^{33}\ P_b \text{ ergs} \quad (6)$$

Six representative flares of the 46 are shown in Figures 6–11. All of the flares shown were acquired at 500 samples/sec. The upper frame of each figure is the actual data plotted with the data at 2-ms intervals. The lower frame is the FFT for the data span shown in the flare plot. Several of the sequences have very evident QPPs, as evidenced in Figures 6, 8, 9, and 11. Those QPPs can be identified in the photon plots and in the FFT for each flare sequence. Figure 12 compiles the peak FFT frequencies from the six data groups. Figure 13 slices the same data by period. From these data the greatest QPP activity is in the 12 Hz and lower frequencies, with equivalent periods generally below 0.1 second.

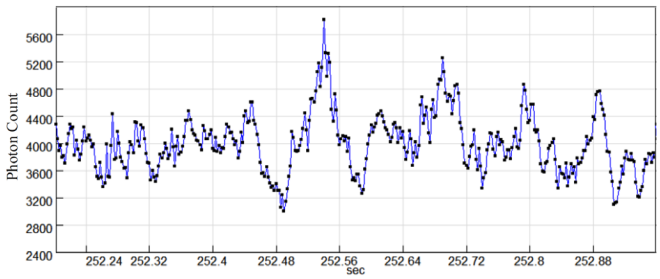

Figure 6a. 1/14/2019, flare 2-3.3 photon count versus seconds: mean 4123, 62 ms, peak 252.54 sec, 5812 photon counts.

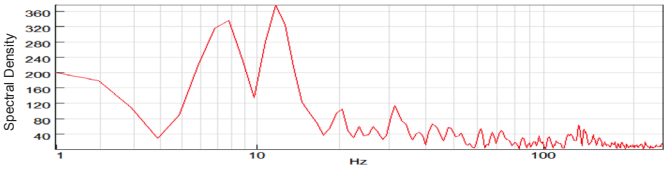

Figure 6b. Relative power spectral density versus frequency; FFT peaks 1.9, 7.8, 11.7. 20.5, and 31.3 Hz.

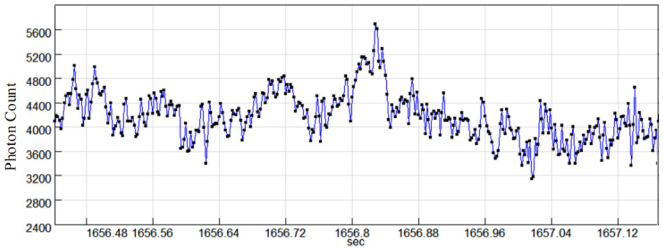

Figure 7a. 1/14/19, flare1-1.1, photon count versus seconds: mean 4183, 48 ms, peak 1656.828 sec, 5692 photon counts.

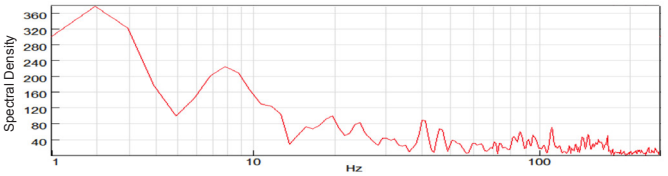

Figure 7b. Relative power spectral density versus frequency; FFT peaks 1.9, 7.8, 20.5, and 40 Hz.

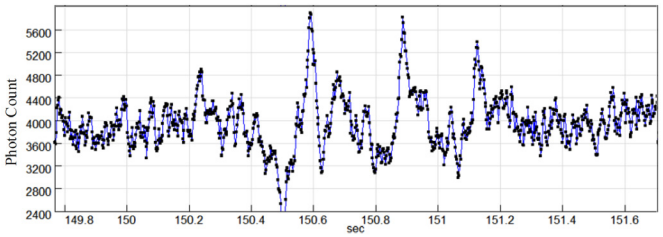

Figure 8a. 1/14/2019, files 8-2.11-4.11, photon count versus seconds: mean 4015, 3 events, peaks 150.59 sec, 72 ms, 5899 photon counts; 150.886 sec, 102 ms, 5817 photon counts; 151.126 sec, 44 ms, 5391 photon counts.

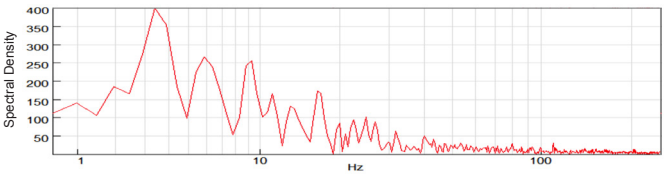

Figure 8b. Relative power spectral density versus frequency; FFT peaks 3.4, 5.9, 9.3, 11.2, 13.2, and 16.6 Hz.

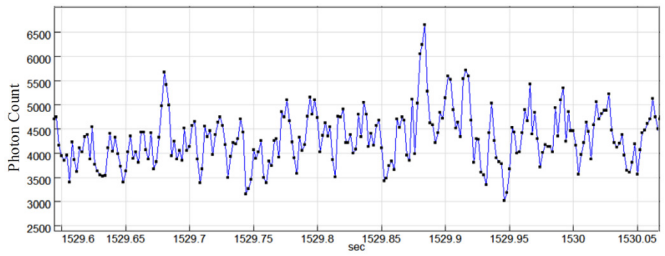

Figure 9a. 1/22/2019, flare 1-2.2, photon count versus seconds: mean 4069, 46 ms, peak 1529.884 sec, 6658 photon counts.

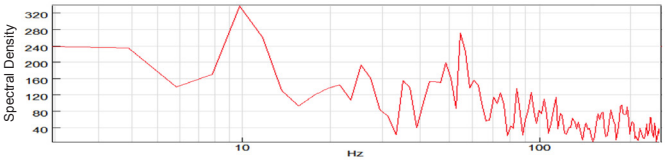

Figure 9b. Relative power spectral density versus frequency; FFT peaks 3.9, 9.8, 25.3, and 54.7 Hz.

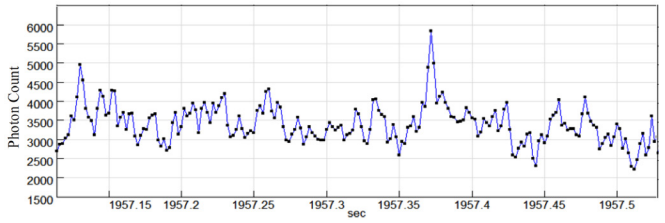

Figure 10a. 4/9/2019, flare 1-3.3, photon count versus seconds: mean 2985, 80 ms, peak 1957.375 sec, 5829 photon counts.

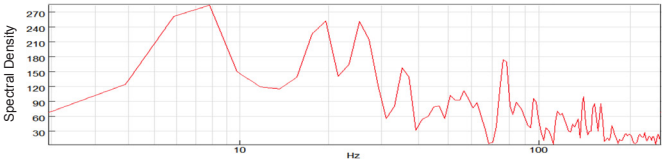

Flare 10b. Relative power spectral density versus frequency; FFT peaks 5.9, 7.8, 19.5, 25.4, 35.2, and 76.2 Hz.

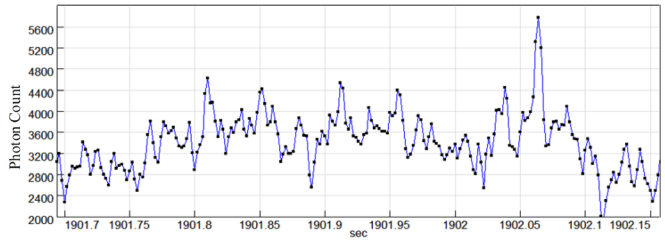

Figure 11a. 4/9/2019, flare 3-2.2, photon count versus seconds: mean 2992, 90 ms, peak 1902.064 sec, 5775 photon counts.

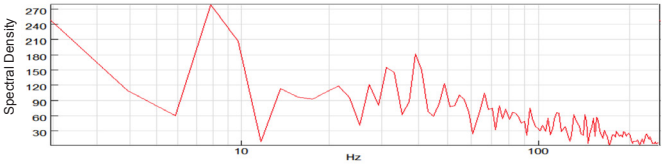

Figure 11b. Relative power spectral density versus frequency; FFT peaks 1.9, 7.8, 9.8, 13.7, 21.5, 31.3, 39.1, and 48.8 Hz.

The search for longer duration flares was undertaken by resampling all the high-speed data into 5-second integration bins and replotted. This improves the S/N and greatly enhances the ability to detect slower outbursts. No flares other than those already noted were identified.

A method of quantifying the activity of flare stars was introduced by Gershberg (1972) and Lacy, Moffett, and Evans (1976). The process develops a cumulative flare frequency distribution diagram of log f of the flare frequency for energy E_1 or greater verses log E. The number (N) of flare energy levels from E_1 to E_{max} is summed and repeated for successive higher values of E. These data are plotted against the flaring frequency, f = N/t, where t is the total monitoring time in hours. The flare data of Table 1 were plotted in the cumulative flare frequency distribution diagram for 47 Cas (Figure 14). The resultant power-law plot significantly reduces random variations and shows a linear relationship until the knee at –0.1 to 0.0 log f. The nonlinearity at higher flare rates is generally due to the system detection threshold at lower energy levels. A similar discontinuity can occur at higher energy levels as the maximum flare energy level is reached for the star. The power-law fit (Lacy, Moffett, and Evans 1976) for flaring activity has the general form of $\log f = \alpha + \beta \log E_b$. Solving using the flare data, $\alpha = 116.43$ and $\beta = -3.548$. The power-law trend line is plotted in Figure 14 along with the cumulative distribution and shows good correlation up to the knee.

4. Summary

X-ray star 47 Cas proved to be a highly energetic optical flare star with a flare rate of 4.6 flares / hr during the 500 s/sec data collection period. This represents a flare rate minimally 100 times that reported on other short duration or spike flare studies. The mechanisms are unknown since no published work has been found on simultaneous X-ray and fast cadence photometry. Of further importance were the numerous QPPs present ranging in frequency from sub-hertz to 25 Hz and above accompanying many of the flare sequences. Quasi-periodic pulses (QPPs) or quasi-periodic oscillations (QPOs) are largely interchangeable terms due to their loose definition. QPPs have been observed in solar and stellar activity and their mechanisms debated. Balona *et al.* 2015 suggest such mechanisms in stellar super-flares as magnetohydromagnetic forces acting on flare loops or acoustic oscillations from high energy particle impulses or quakes but little conclusive evidence, concluding that "new processes need to be found." Warner and Woudt (2008) discuss QPOs in CVs, citing possible mechanisms but with no applicable conclusions. Furthermore, the type of QPPs seen in 47 Cas are different from those cited; they are higher frequency, occur with great rapidity and amplitude, and are part of the actual flare sequence in many cases. A definitive QPP mechanism is currently unknown. Future availability of concurrent data at X-ray, radio, and optical wavelengths may help answer the causal factors for such phenomena along with improved modeling of star systems demonstrating repetitive oscillations or pulses.

The cumulative flare frequency profile followed well the typical relationship for flaring activity.

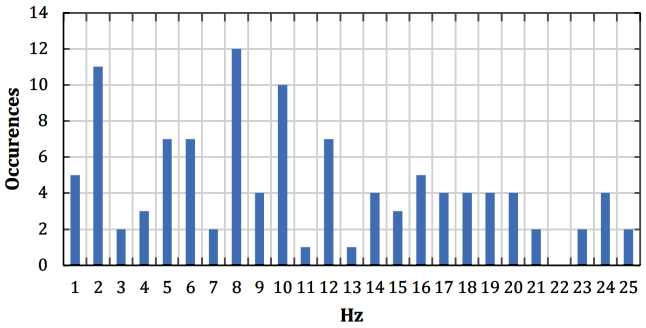

Figure 12. FFT data of occurrences versus frequency compiled from Figures 6–11.

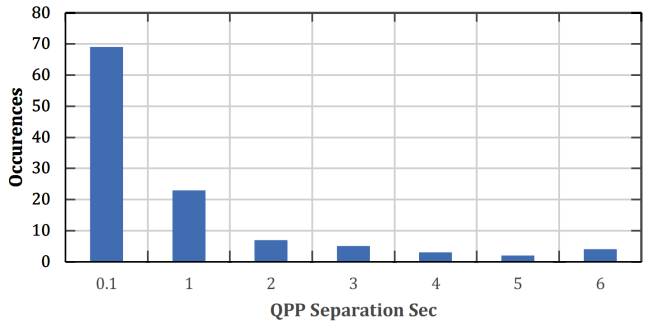

Figure 13. FFT data from Figures 6–11 converted to equivalent periods.

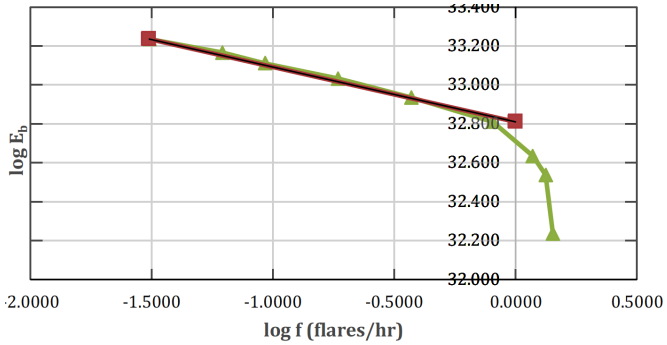

Figure 14. Cumulative B-band flare frequency distribution diagram with trend line, log f = 116.43 – 3.548 log E_b.

5. Acknowledgements

The author expresses his thanks to the referee for probing and questioning in several important areas and Dr. A. Henden for assistance on the 47 Cas quiescent energy calculation. This research has made use of the SIMBAD database, operated at CDS, Strasbourg, France.

References

Astrodon. 2019, Sloan optical filters (https://astrodon.com/products/astrodon-photometrics-sloan-filters).

Balona, L. A., Broomhall, A.-M., Kosovichev, A., Nakariakov, V. M., Pugh, C. E., and Van Doorsselaere, T. 2015, *Mon. Not. Roy. Astron. Soc.*, **450**, 956.

Byrne, P. B., Lanzafame, A. C., Sarro, L. M., and Ryans, R. 1994, *Mon. Not. Roy. Astron. Soc.*, **270**, 427.

Gershberg, R. E. 1972, *Astrophys. Space Sci.*, **19**, 75.

Gudel, M., Guinan, E. F., Etzel, P. B., Mewe, R., Kaastra, J. S., and Skinner, S. L. 1998, in *The Tenth Cambridge Workshop on Cool Stars, Stellar Systems and the Sun*, eds. R. A. Donahue, J. A. Bookbinder, ASP Conf. Ser. 154, Astronomical Society of the Pacific, San Francisco, 1247.

Henden, A. A., and Kaitchuck, R. H. 1990, *Astronomical Photometry*, Willmann-Bell, Richmond, VA.

Hoffleit, D., and Warren, W. H., Jr. 1995, *Bright Star Catalogue*, 5th ed.

Lacy, C. H., Moffett, T. J., and Evans, D. S. 1976, *Astrophys. J., Suppl. Ser.*, **30**, 85.

Measurement Computing. 2019, data acquisition systems (https://www.mccdaq.com/productsearch.aspx?q=daqboard).

Olsen, E. H. 1983, *Astron. Astrophys.*, **54**, 55.

Pandey, J. C., and Karmakar, S. 2015, *Astron. J.*, **149**, 47.

SignalLab. 2019, SIGVIEW 3.2 software for DSP applications (http://www.sigview.com/index.htm).

Vander Haagen, G. A. 2012, in *The Society for Astronomical Sciences 31st Annual Symposium on Telescope Science*, eds. B. D. Warner, R. K. Buchleim, J. L. Foote, D. Mais, Society for Astronomical Sciences, Rancho Cucamonga, CA, 165.

Vander Haagen, G. A. 2013, *J. Amer. Assoc. Var. Star Obs.*, **41**, 320.

Vander Haagen, G. A. 2015, *J. Amer. Assoc. Var. Star Obs.*, **43**, 219.

Vander Haagen, G. A. 2017, *J. Amer. Assoc. Var. Star Obs.*, **45**, 36.

Warner, B., and Woudt, P. A. 2008, in *Cool Discs, Hot Flows: The Varying Faces of Accreting Compact Objects*, AIP Conf. Proc. 1054, AIP Publishing, Melville, NY, 101.

Wenger, M., *et al.* 2000, "The SIMBAD astronomical database" (http://simbad.u-strasbg.fr/simbad) *Astron. Astrophys., Suppl. Ser.*, **143**, 9.